



Crystallization kinetics in $\text{Cu}_{50}\text{Zr}_{42.5}\text{Ti}_{7.5}$ bulk metallic glass

V. A. Bykov¹ · T. V. Kulikova¹ · D. A. Kovalenko¹ · S. Kh. Estemirova¹ · R. E. Ryltsev^{1,2}

Received: 20 July 2023 / Accepted: 17 December 2023 / Published online: 29 February 2024
© Akadémiai Kiadó, Budapest, Hungary 2024

Abstract

The production of modern composite materials based on bulk metallic glasses requires knowledge of their primary crystallization processes during heating (BMG). Here, we investigate the structure and crystallization kinetics of a promising modern BMG/B2 nano-composites, a fast-hardened glass-forming alloy $\text{Cu}_{50}\text{Zr}_{42.5}\text{Ti}_{7.5}$. The complex four-step crystallization of the glass alloy at different heating rates was revealed by differential scanning calorimetry. The process of a crystallization was successfully fully described by a multiverse nonlinear kinetic model, and the kinetic parameters were determined with high accuracy. The best way to describe the four-step crystallization of a glass alloy is the two-branch parallel reaction. The first branch is described by three consecutive n-order autocatalytic reactions. The second branch obeys the Avrami-Erofeev model. The high thermal stability of the amorphous state is evidenced by the average full process crystallization activation energy $E_a = 425 \text{ kJ mol}^{-1}$. Analysis of the obtained results and their comparison with available literature data allow us to conclude that the crystallization process in glassy $\text{Cu}_{50}\text{Zr}_{42.5}\text{Ti}_{7.5}$ alloy (and probably other similar ternary alloys based on binary $\text{Cu}_{50}\text{Zr}_{50}$ system) is strongly affected by the structure of initial sample as well as by thermal conditions. The presence of nano-sized inclusion of metastable phases (for example, B2 one) can change the sequence of reaction as well as the structure of phases forming at each stage.

Keywords Crystallization kinetics · Growth models · X-ray diffraction · Bulk metallic glasses

Introduction

In the last few decades, bulk metallic glasses (BMGs) have been intensively experimentally and theoretically investigated due to their unusual physical properties and the possibility of commercial applications [1–6]. However, BMGs are not used as structural materials because they have poor tensile and fracture toughness properties [7–10]. The drawback of poor mechanical properties of BMGs can be solved by obtaining composites with a BMG matrix. The ductility and compressive toughness [11, 12] of a composite with a BMG matrix are significantly higher than those of the original BMG alloy.

The development of this direction in the synthesis of composites with BMG matrix allowed to create a new type of high-strength plastic composites BMG on the basis of CuZr [13, 14]. Cu-Zr system is one of the few binary systems forming BMG [15–17]. The glass-forming ability and thermal stability of the resulting BMG Cu-Zr alloys were significantly improved by the addition of Al, Ti, and others. It was previously established [16, 18, 19] that the formation of BMG in Cu-Zr alloys occurs in narrow concentration intervals. The $\text{Cu}_{50}\text{Zr}_{50}$ alloy forms BMG and also exhibits shape memory effects due to the reversible martensitic transformation (MT) of the B2 CuZr intermetallide [20]. Due to the presence of MT, it is possible to form a high-strength ductile composite based on $\text{Cu}_{50}\text{Zr}_{50}$ alloy. Since the shape memory phase B2 CuZr is plastic, by placing it in a glassy matrix at rapid solidification, it is possible to obtain samples with excellent mechanical properties [21, 22]. Obviously, the most promising candidates for the formation of such composites [23] are ternary alloys close in composition to $\text{Cu}_{50}\text{Zr}_{50}$.

Knowledge of the mechanisms of crystallization kinetics makes it possible to obtain BMG/B2 composites with

✉ D. A. Kovalenko
darya.k.2000@list.ru

¹ Ural Federal University, Mira Str. 19, Yekaterinburg, Russia 620002

² Institute of Metallurgy, Ural Division of Russian Academy of Sciences, Amundsena Str. 101, Yekaterinburg, Russia 620016

specified properties. Cu-Zr-based BMG alloys often crystallize in several stages, which makes it difficult to interpret the crystallization mechanism as a whole. In addition, the mechanism of formation of Cu-Zr-based BMG nano-crystalline phase is not fully understood. Here, the subject of our studies is $\text{Cu}_{50}\text{Zr}_{42.5}\text{Ti}_{7.5}$ alloy, which exhibits the best glass-forming ability among Cu-Zr-Ti alloys near $\text{Cu}_{50}\text{Zr}_{50}$ [24, 25]. We comprehensively study the crystallization kinetics in $\text{Cu}_{50}\text{Zr}_{42.5}\text{Ti}_{7.5}$ sample using differential scanning calorimetry (DSC), X-ray diffraction analysis (XRD), and model kinetic analysis techniques. Summarizing the experimental data, we introduce a multiverse nonlinear kinetic model, which fully describes the crystallization process and allows us to determine the kinetic parameters with high accuracy.

Experimental procedure

The $\text{Cu}_{50}\text{Zr}_{42.5}\text{Ti}_{7.5}$ alloy was made from copper, zirconium, and titanium with a purity of 99.98 mass%. Further, the alloy components were placed in an arc furnace and remelted at least five times in helium atmosphere. The major impurities and the nominal alloy composition were checked on a Spectroflame Modula S atomic emission analyzer.

The vacuum casting method realized in an arc furnace was used to produce BMG samples with a diameter of 3 mm. The calculated cooling rate was 300–400 K/s. A Shimadzu XRD-7000 X-ray diffractometer was used for structural analysis of amorphous samples. Cu-K α radiation, angle range, 0.03 degree step, 4 s scanning step, graphite monochromator, and silicon powder as an external standard were the experimental conditions on the X-ray analyzer. Phase identification was carried out using the International Centre for Diffraction Data (ICDD) PDF-2 database.

Thermal reactions in the sample were investigated by differential scanning calorimetry using a Netzsch STA 449C device, calibrated with indium, tin, zinc, aluminum, silver, and gold standards. The selected sample mass was $20.1 \pm 0.1 \cdot 10^{-6}$ kg. Kinetic analysis was carried out using the Netzsch Thermokinetics package.

Results

Before starting the kinetic analysis, we performed XRD analysis to ensure that the suction-cast samples were completely amorphous. In Fig. 1, we show the corresponding XRD pattern, which reveals the halo characteristic of amorphous materials; no crystalline peaks are observed.

To estimate the kinetic parameters of the crystallization process of the $\text{Cu}_{50}\text{Zr}_{42.5}\text{Ti}_{7.5}$ sample, DSC measurements were taken in the temperature range from 20 to 600 °C at different heating rates (2, 5, 10, 16, 23 K min $^{-1}$) (Fig. 2)

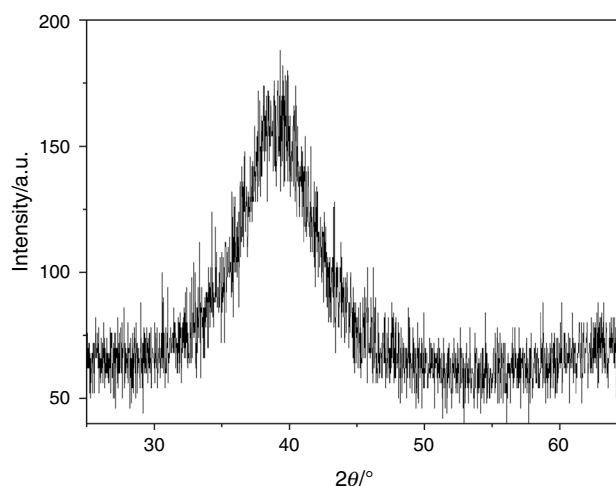


Fig. 1 XRD pattern of $\text{Cu}_{50}\text{Zr}_{42.5}\text{Ti}_{7.5}$ amorphous alloy obtained by suction-casting method

at an argon flow of 60 mL mol $^{-1}$. There are four exothermic calorimetric effects on the DSC curves corresponding to crystallization processes; all of them will be considered when constructing the kinetic model. Note that all DSC curves reveal a well-defined endothermic peak corresponding to reversion, and the corresponding glass transition temperature T_g is substantially lower than the primary crystallization temperature. This fact agrees with the high glass-forming ability of the alloy. Indeed, the critical diameter of the amorphous suction-cast rods is 5 mm [24, 25]. The values of characteristic temperatures (such as the glass transition temperature T_g , the onset crystallization temperature T_x , the peak temperatures T_{p1} , T_{p2} , T_{p3} , T_{p4} , and the super-cooled liquid region $\Delta T = T_x - T_g$) for $\text{Cu}_{50}\text{Zr}_{42.5}\text{Ti}_{7.5}$ BMG are shown in Table 1.

Before performing the model kinetic analysis, we evaluated the kinetic parameters, pre-exponential factor A , and the activation energy E_a using model-free methods, such as the Kissinger, Ozawa–Flynn–Wall, and Friedman methods [26, 27]. The results of the calculation of the kinetic parameters using these methods are presented in Tables 2 and 3. We see from Table 2 that the kinetic parameters obtained using the different methods demonstrate large dispersion. The reason for this is that the crystallization process in the alloy under investigation is very complex and so model-free methods provide only a rough estimation.

We can roughly estimate the average activation energy for the amorphous $\text{Cu}_{50}\text{Zr}_{42.5}\text{Ti}_{7.5}$ sample as $E_a \approx 425$ kJ mol $^{-1}$. This value is quite typical for Cu-Zr-based BMGs. The kinetic parameters obtained using model-free methods are used as initial values in the model analysis.

To describe the crystallization processes in the $\text{Cu}_{50}\text{Zr}_{42.5}\text{Ti}_{7.5}$ sample, kinetic modeling was performed using the multivariate nonlinear regression method. In the

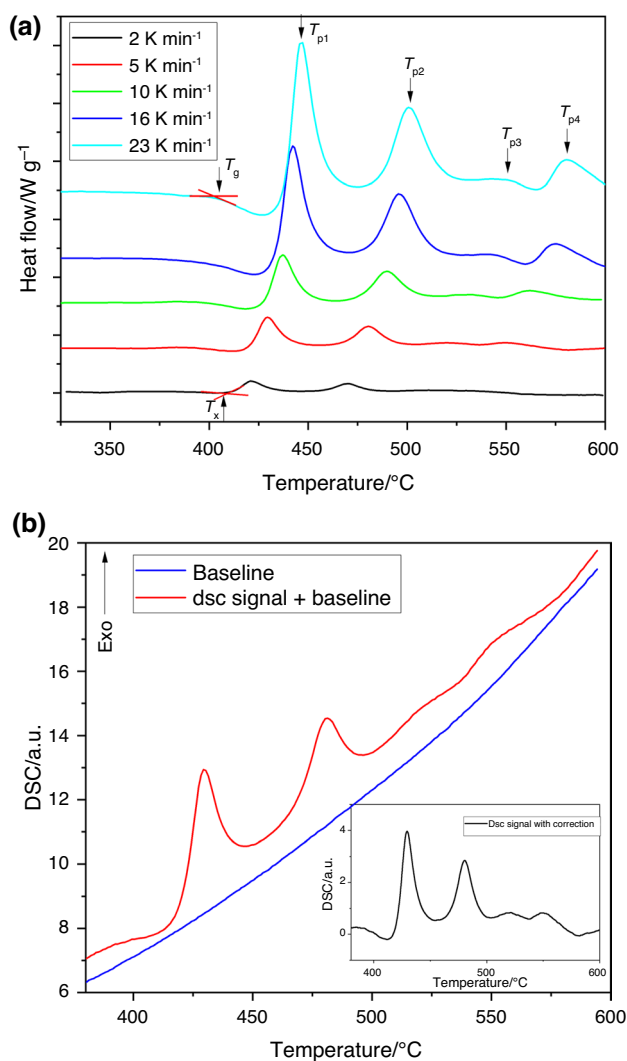


Fig. 2 **a** Experimental DSC curves of Cu₅₀Zr_{42.5}Ti_{7.5} amorphous alloy obtained at different heating rates, **b** DSC curve at 5 K min⁻¹ to confirm the existence of four peaks (inset: DSC curve + correction)

framework of this method, a kinetic reaction model is constructed (sequential, parallel, branched, etc.), and each stage is described using a certain kinetic differential equation (Avrami-Erofeev, Prout-Tomkins, etc.). Such equations contain many parameters that are determined by the nonlinear regression method by fitting the experimental DSC curves.

Table 1 Characteristic temperatures of Cu₅₀Zr_{42.5}Ti_{7.5} BMG measured at different heating rates

Heating rate, K/min	$T_g/^\circ\text{C}$	$T_x/^\circ\text{C}$	$T_{p1}/^\circ\text{C}$	$T_{p2}/^\circ\text{C}$	$T_{p3}/^\circ\text{C}$	$\Delta T/^\circ\text{C}$
2	397.9	412.7	421.3	469.9	529.6	14.8
5	400.8	418.8	429.5	480.5	549.3	18
10	401.7	426.1	437.2	489.8	562.2	24.4
16	406	430.4	442.2	495.9	575.1	24.4
23	416.5	435.2	446.5	500.7	580.6	18.7

The experimental DSC curves of the crystallization process of the Cu₅₀Zr_{42.5}Ti_{7.5} alloy were described by different multivariate nonlinear regression models. It was found that best correlation coefficient (0.998) between the measured and simulated curves (Fig. 3a, b, c) is achieved by the scheme of two-branch parallel reaction:



The first three stages (A → B), (B → C), and (C → D) are described by a heterogeneous reaction with n-order autocatalysis

$$\frac{d\alpha}{dt} = k\alpha^n(1 + k_{\text{cat}}\beta) \quad (2)$$

where k_{cat} is the autocatalysis coefficient. Hereinafter, $k(T) = \exp(Ea/RT)$ is the reaction rate constant, obeying the Arrhenius law; α is the concentration of the initial substance; β is the concentration of the reaction product; t is the time; T is the temperature.

The second one-step branch (A → E) obeys Avrami-Erofeev model

$$\frac{d\alpha}{dt} = kn(1 - \alpha)(-\ln(1 - \alpha))^{(n-1)/n} \quad (3)$$

In Fig. 3a, we compare the DSC curves of the alloy obtained by experiment and using kinetic model. We observed rather good fitting of the experimental curves by the modeled curves; the correlation coefficient of the fit was 0.9926.

Table 4 shows the kinetic parameters and regression coefficient R2 for the multivariate nonlinear regression fitting based on a two-branch parallel process.

To verify the obtained kinetic model, we performed complete structural analysis at each stage of the crystallization process. The glassy sample was heated to a target temperature, annealed isothermally for a certain time τ , and then cooled to room temperature. Note that the thermal conditions of XRD measurements differ from those used in the kinetic DSC measurements and so the temperatures corresponding to the phase transformations do not match

Table 2 Kinetic parameters of crystallization process of $\text{Cu}_{50}\text{Zr}_{42.5}\text{Ti}_{7.5}$ amorphous alloy estimated by Ozawa–Flynn–Wall and Friedman methods

Method	$E_a/\text{kJ}\cdot\text{mol}^{-1}$	$\log A/\text{s}^{-1}$
Ozawa–Flynn–Wall	400	26.5
Friedman	450	28
Average	425	27.25

Table 3 Activation energy (E_a) and frequency factor ($\log A$) derived by Kissinger method

	1st peak	2nd peak	3rd peak	4th peak
$E_a/\text{kJ mol}^{-1}$	364	361	237	307
$\log A/\text{s}^{-1}$	24.5	22.9	17.7	17.7

exactly. However, the consequences of transformations in both cases should be the same. According to XRD, the glass phase does not crystallize in the temperature range of $T =$

445–450 °C through annealing treatment. At the same time, a noticeable narrowing of the amorphous halo profile was observed (Fig. 4). This indicates a change in the local order with the possible formation of nano-sized crystalline nuclei. After further heating to $T = 470$ °C, the XRD patterns reveal the beginning of the crystallization process (Fig. 5). We see XRD peaks corresponding to cubic (Pm-3m) and orthorhombic (C2ca) phases. Very large width of the diffraction maxima at small angles suggests the small size of crystallites. Besides the crystalline phases, the sample still contains an amorphous phase, as indicated by an increased diffuse background. At $T = 530$ °C, the X-ray diffraction peaks of the orthorhombic and cubic phases become narrower, and the background fluctuations decrease. At $T = 550$ °C, the sample contains a tetragonal (s. g. I4/mmm) crystalline phase along with orthorhombic and cubic phases. The peaks of the detected crystalline phases become narrower, indicating the growth of crystallites. Only orthorhombic and tetragonal phases were detected at $T = 580$ and $T = 600$ °C; the cubic phase is not found. Thus, the three-phase region is formed in a narrow temperature range of 530–580 °C.

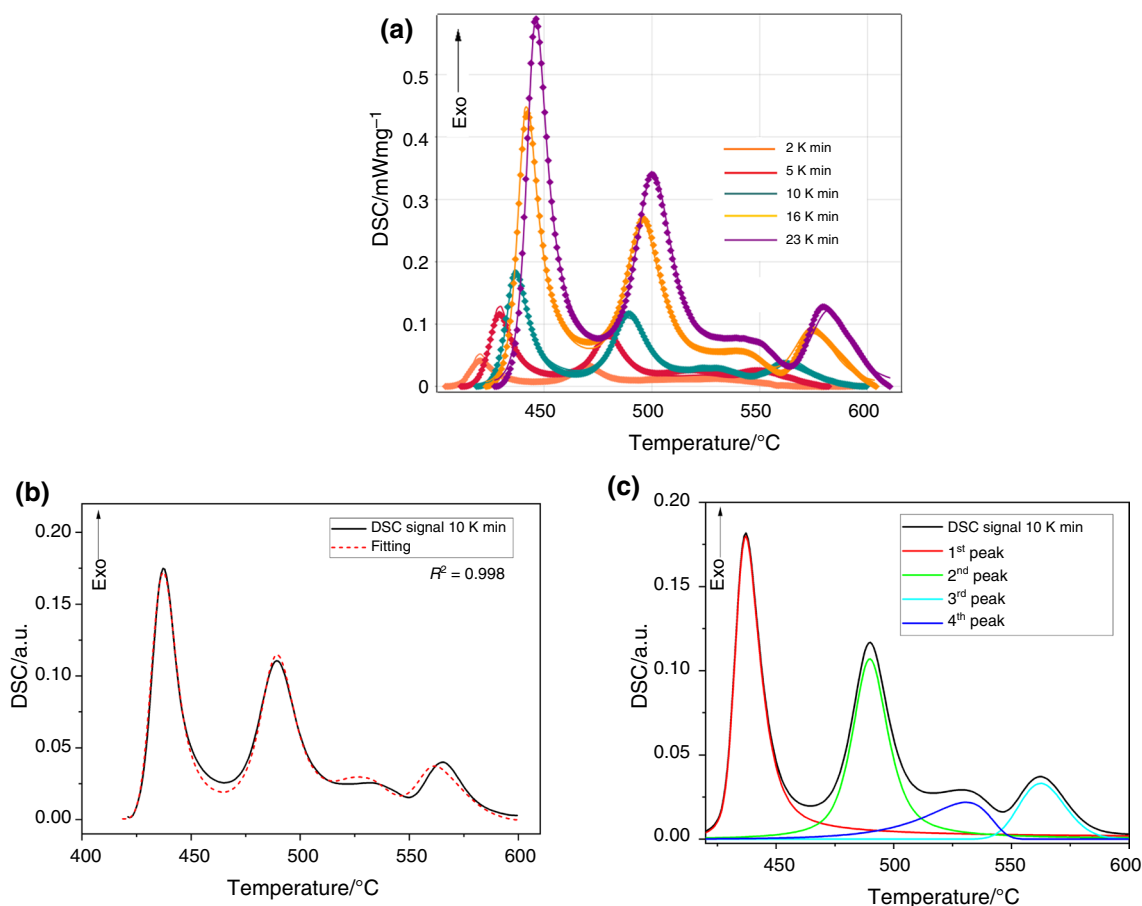
**Fig. 3** **a** DSC curves of BMG $\text{Cu}_{50}\text{Zr}_{42.5}\text{Ti}_{7.5}$ alloy: obtained (dots) experiment and (solid lines) kinetic model, **b** comparison of experimental and calculated fit at 10 K min⁻¹, **c** deconvolution of DSC curves for a heating rate of 10 K/min

Table 4 Kinetic parameters of crystallization process of $\text{Cu}_{50}\text{Zr}_{42.5}\text{Ti}_{7.5}$ amorphous alloy (n —reaction order, $\log A$ —pre-exponential factor, E_a —activation energy, R^2 —coefficient of correlation) obtained by nonlinear regression kinetic model

$n_{A \rightarrow B}$	$n_{B \rightarrow C}$	$n_{C \rightarrow D}$	$n_{A \rightarrow E}$	$\log A_{A \rightarrow B}, \log/s^{-1}$	$\log A_{A \rightarrow B}, \log/s^{-1}$	$\log A_{A \rightarrow B}, \log/s^{-1}$	$E_{a, A \rightarrow B}, \text{kJ mol}^{-1}$	$E_{a, B \rightarrow C}, \text{kJ mol}^{-1}$	$E_{a, C \rightarrow D}, \text{kJ mol}^{-1}$	$E_{a, A \rightarrow E}, \text{kJ mol}^{-1}$	R^2	
3.5	2.3	1.9	1.3	24.3	21.6	13.9	26.2	372.4	352.6	272.8	437.5	0.998

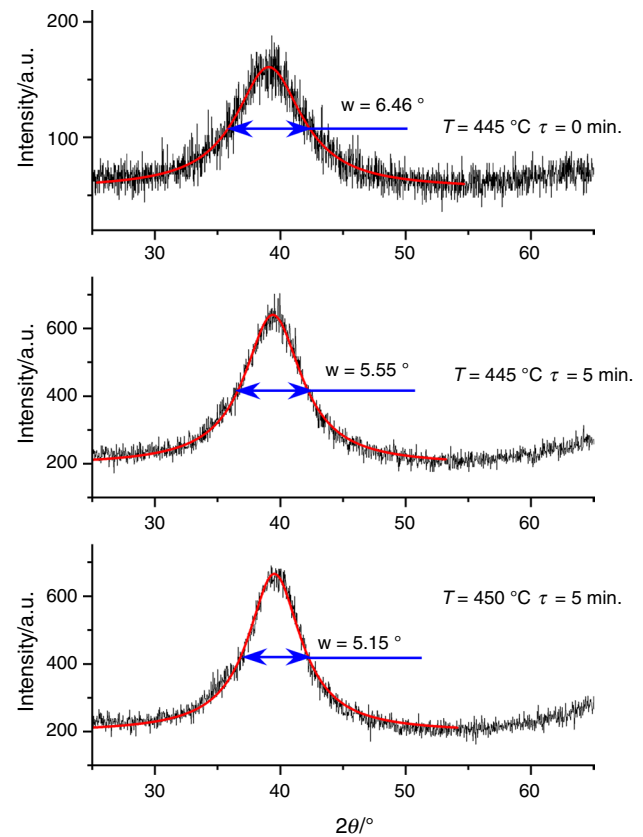


Fig. 4 XRD pattern of $\text{Cu}_{50}\text{Zr}_{42.5}\text{Ti}_{7.5}$ bulk metallic glass subjected to heat treatment below the crystallization temperature

Probably, the tetragonal phase is the result of a phase transformation from the cubic phase.

Thus, according to XRD analysis, the crystallization of $\text{Cu}_{50}\text{Zr}_{42.5}\text{Ti}_{7.5}$ bulk metallic glass begins above $T = 450^\circ\text{C}$ and proceeds in three stages. In the first stage of crystallization, we have nano-sized crystallites of two phases with orthorhombic and cubic crystal structures. These phases coexist in the temperature range of $470\text{--}530^\circ\text{C}$; crystallites of both phases increase with increasing temperature. The second stage covers a narrow temperature range between 530 and 580°C and is characterized by the coexistence of three phases: orthorhombic, cubic, and tetragonal. In the third stage, crystallization process ends with the formation of two phases with orthorhombic and tetragonal symmetries. Comparison of the results obtained with the literature data [28] on the structure of the Cu-Zr-Ti phases allows us to conclude that the cubic Pm-3m phase corresponds to the B2 CuZr phase, the orthorhombic (C2ca) phase corresponds to the $\text{Cu}_{10}(\text{Zr}_{1-x}\text{Ti}_x)_7$ solid solution, and the tetragonal phase (I4/mmm) to the $\text{Cu}(\text{Zr}_{1-x}\text{Ti}_x)_2$ solid solution.

To obtain additional insight into the structure of the system, we performed microstructural analysis of the annealed sample using a Carl Zeiss EVO 40 microscope equipped

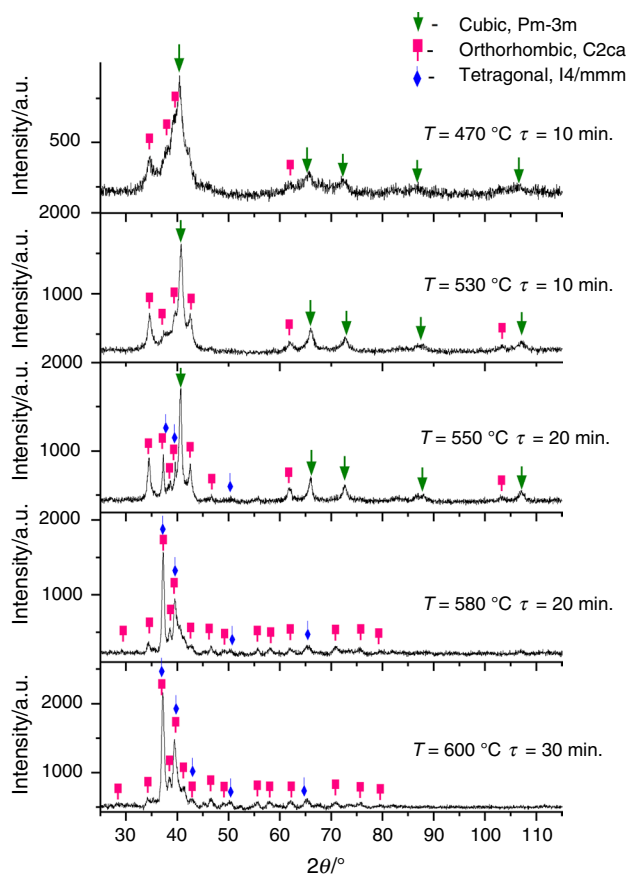


Fig. 5 XRD pattern of $\text{Cu}_{50}\text{Zr}_{42.5}\text{Ti}_{7.5}$ bulk metallic glass subjected to heat treatment above the crystallization temperature

with an INCAEnergy EDS X-ray microanalysis analyzer (EDX). The specimen was heated to 650 °C and the annealing time was 1 hour. According to microstructural analysis, only two phases were found in the alloy structure (see Fig. 6a). These are orthorhombic (s.g. C2ca) and tetragonal (s.g. I4/mmm) crystalline phases.

Using backscattered electron imaging, microstructural characterization of the sample during annealing verified that the alloy is homogenous both chemically and structurally (Fig. 6b). The element scanning does not reveal areas enriched in one of the constituent metals.

Discussion

Above, we have reported the results of the kinetic analysis of crystallization in $\text{Cu}_{50}\text{Zr}_{42.5}\text{Ti}_{7.5}$ bulk metallic glass and the structural examination of the samples at different stages of the crystallization process. Here, we discuss the obtained results in the context of available literature data and propose a consistent picture of the crystallization process.

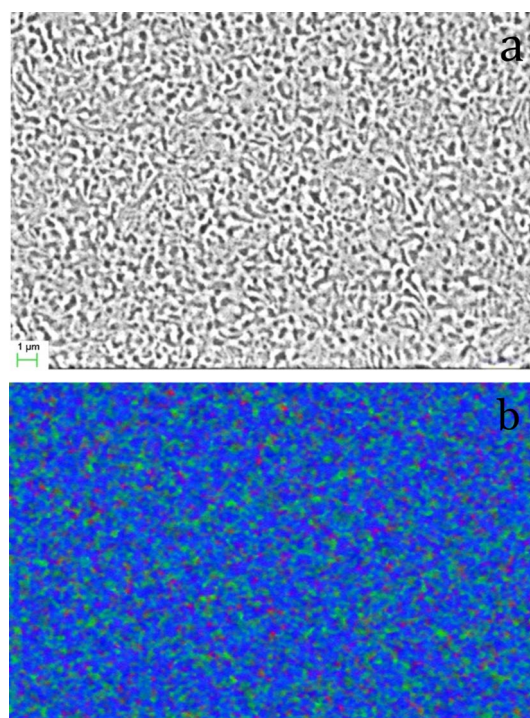


Fig. 6 SEM images of $\text{Cu}_{50}\text{Zr}_{42.5}\text{Ti}_{7.5}$ bulk metallic glass annealed (crystallized) at $T = 650$ °C for 1 h. **a** Backscattered electron image, **b** element mapping

We start our discussion with the analysis of the crystallization in the binary $\text{Cu}_{50}\text{Zr}_{50}$ system, which is the basis for many Cu-Zr-TM glass-forming alloys designed by the small addition of transition metals. Such alloys often demonstrate similar behavior to the base binary system. There are many studies in which authors addressed the crystallization process in $\text{Cu}_{50}\text{Zr}_{50}$ glasses (see [29] and references therein). For example, a comprehensive analysis of the phase evolution sequence during devitrification of $\text{Cu}_{50}\text{Zr}_{50}$ metallic glass is made in Ref. [29]. It was revealed that continuous heating of the glassy sample causes simultaneous formation of orthorhombic $\text{Cu}_{10}\text{Zr}_7$, tetragonal CuZr_2 (C11b), and cubic CuZr (B2), followed immediately by the dissolution of the CuZr (B2) phase. Experimental conditions did not allow them to differentiate the initial crystallization event and resolve the formation of individual phases. However, it is more likely that the primary crystallization event is associated with the formation of the metastable but kinetically favored B2 phase, which decomposes into equilibrium $\text{Cu}_{10}\text{Zr}_7$ and CuZr_2 phases.

The crystallization process in ternary Cu-Zr-Ti alloys is much more complicated and substantially depends on Ti concentration as well as on the initial structure of the sample and the heating conditions [30–32]. For example, it is reported in Ref. [30] that heating of $\text{Cu}_{50}\text{Zr}_{42.5}\text{Ti}_{7.5}$ amorphous ribbons resulted in three-stage transformation: glass

→ nano-crystals → CuZrTi (C15) + $\text{Cu}_{10}\text{Zr}_7$ → $\text{Cu}_{10}\text{Zr}_7$ + CuZr_2 . Here, CuZrTi is a metastable ternary phase with the structure of C15 Laves phase. This phase is not among equilibrium ones for $\text{Cu}_{50}\text{Zr}_{42.5}\text{Ti}_{7.5}$ alloy, but it was reported as a stable phase in another region of the phase diagram [33]. It is important that the final state of the crystallization process is a two-phase state: $\text{Cu}_{10}\text{Zr}_7$ + CuZr_2 . This contradicts to the most recent assessments of Cu-Zr-Ti phase diagram [22, 28] where the equilibrium state for $\text{Cu}_{50}\text{Zr}_{42.5}\text{Ti}_{7.5}$ alloy at $T < 994$ K contains three phases: $\text{Cu}_{10}\text{Zr}_7$, CuZr_2 , and ternary Cu_2ZrTi (τ_1) phase with the structure of the C14 Laves phase. Another picture is reported in Refs. [31, 32] where suction-casted $\text{Cu}_{50}\text{Zr}_{42.5}\text{Ti}_{7.5}$ samples were revealed as a glassy matrix with inclusions of CuZr (cubic B2 and/or monoclinic martensitic) and/or $\text{Cu}_{10}\text{Zr}_7$ phases depending on the cooling rate (diameter of the rods).

The results obtained here differ from those mentioned above. First, the initial state of our sample is completely X-ray amorphous; no traces of crystalline inclusions were detected. However, the autocatalytic process of the crystallization process suggests that nano-inclusions of the B2 phase, which are undetectable by XRD, can occur in the suction-casted sample. The contradiction with the results obtained in Refs. [31, 32] where similar mold diameters were utilized can be explained by different cooling conditions caused by differences in suction-casting equipment. The presence of nano-sized inclusions of B2 phase can explain the growth of this phase at the initial stage of the crystallization process despite metastability of this phase.

Second, we did not observe the presence of the ternary Laves phase at the final stage of the crystallization process. This agrees with the results reported in Ref. [30] but contradicts Refs. [28, 34] and thus raises issues regarding the phase diagram of Al-Cu-Ti alloys. Moreover, we did not observe any ternary (Laves) phase during the intermediate stages of the crystallization process. However, considering that XRD analysis does not reveal one of the crystallization stages detected by DSC, we argue that the metastable Laves phase forms at the stage B → C in accordance with the reaction scheme (Fig. 7). The question of what type of Laves phase (C14, C15) occurs in our case is still open. It is known that different Laves polytypes have similar local structure and so are expected to have very close energies and can demonstrate strong competition during crystallization [35]. This situation is well-known in binary and ternary alloys, and it is reasonable to expect that contradiction between different literature data and our results is a consequence of this competition.

Thus, by analyzing our results and comparing them with the literature data, we suggest the following sequence of transformations during the crystallization of $\text{Cu}_{50}\text{Zr}_{42.5}\text{Ti}_{7.5}$ bulk metallic glass (see Fig. 7): The first stage of the

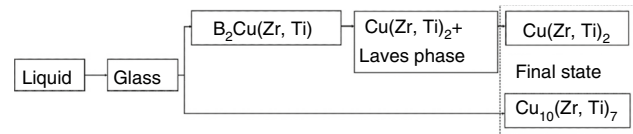


Fig. 7 The scheme demonstrating the sequence of transformations during crystallization of $\text{Cu}_{50}\text{Zr}_{42.5}\text{Ti}_{7.5}$ bulk metallic glass

crystallization process (A → B) corresponds to the formation of the metastable B2 Cu(Zr, Ti) phase, which then partially decomposes into the metastable Laves phase (C14 or C15) and finally transforms into the stable $\text{Cu}(\text{Zr}_{1-x}\text{Ti}_x)_2$, whereas the parallel reaction A → E corresponds to the nucleation and growth of $\text{Cu}_{10}(\text{Zr}_{1-x}\text{Ti}_x)_7$ solid solution.

Conclusions

For the first time, a kinetic model of the crystallization process in $\text{Cu}_{50}\text{Zr}_{42.5}\text{Ti}_{7.5}$ bulk metallic glass alloy was constructed using an integrated approach that includes calorimetric studies, X-ray phase analysis, electron microscopy, and kinetic modeling by multivariate nonlinear regression. It was found that the crystallization of the alloy proceeds as a multistep two-branch parallel reaction. The first branch is described by three sequential n-order autocatalytic reactions, the second obeys Avrami-Erofeev model. The activation energy of the primary crystallization of the alloy was estimated to be $E_a = 425$ kJ mol⁻¹; a high value of E_a indicates the stability of the amorphous state.

Analysis of the obtained results and their comparison with available literature data allow us to conclude that the crystallization process in glassy $\text{Cu}_{50}\text{Zr}_{42.5}\text{Ti}_{7.5}$ alloy (and probably other similar ternary alloys based on binary $\text{Cu}_{50}\text{Zr}_{50}$ system) is strongly affected by the structure of initial sample as well as by thermal conditions. The presence of nano-sized inclusion of metastable phases (for example, B2 one) can change the sequence of reaction as well as the structure of phases forming at each stage. In particular, the formation of metastable ternary Laves phases with different symmetries can substantially affect the crystallization process at both intermediate and final stages of the crystallization process. We suggest that this fact can explain contradictions between different data, including the phase diagram of Cu-Zr-Ti system in the range of compositions around the studied one.

Acknowledgements The research funding from the Ministry of Science and Higher Education of the Russian Federation (Ural Federal University Program of Development within the Priority-2030 Program) is gratefully acknowledged. Experiments were taken using scientific instruments included in the Shared Equipment Center "Ural-M".

References

- C. Suryanarayana, A. Inoue. (2010) Bulk metallic glasses. CRC Press
- Trexler MM, Thadhani NN. Mechanical properties of bulk metallic glasses. *Prog Mater Sci.* 2010. <https://doi.org/10.1016/j.pmatsci.2010.04.002>.
- Wang W, Dong C, Shek C. Bulk metallic glasses. *Mater Sci Eng R.* 2004. <https://doi.org/10.1016/j.mser.2004.03.001>.
- Tao Xu, Wang X, Yuxuan Tu, Zhuo L, Jian Z. Comparing the formation, properties and structure between $\text{Fe}_{20}\text{Co}_{20}\text{Ni}_{20}\text{Cr}_{20}(\text{P}_{0.45}\text{B}_{0.2}\text{C}_{0.35})_{20}$ high-entropy metallic glass and the predecessor $\text{Fe}_{75}\text{Cr}_5\text{P}_9\text{B}_4\text{C}_7$ metallic glass. *J Mater Res Technol.* 2023;26:8289–97.
- Tao Xu, Yao J, Zhuo L, Jie Z. Tuning non-isothermal crystallization kinetics between $\text{Fe}_{20}\text{Co}_{20}\text{Ni}_{20}\text{Cr}_{20}(\text{P}_{0.45}\text{B}_{0.2}\text{C}_{0.35})_{20}$ high-entropy metallic glass and the predecessor $\text{Fe}_{75}\text{Cr}_5\text{P}_9\text{B}_4\text{C}_7$ metallic glass. *Metals.* 2023;13:1624.
- Tao Xu, Zhang L, Li X, Zhuo L, Li G, Jie Z, Jian Z. Adjusting non-isothermal crystallization kinetics through similar solute element Ga microalloying for Al in novel La-Al-C metallic glasses. *J Therm Anal Calorim.* 2022;147(21):12231–43.
- Yavari AR, Lewandowski JJ, Eckert J. Mechanical properties of bulk metallic glasses. *MRS Bull.* 2007. <https://doi.org/10.1557/mrs2007.125>.
- Greer AL. Metallic glasses on the threshold. *Mater Today.* 2009. [https://doi.org/10.1016/S1369-7021\(09\)70037-9](https://doi.org/10.1016/S1369-7021(09)70037-9).
- Yang B, Liu C, Nieh T, Morrison M, Liaw P, Buchanan R. Localized heating and fracture criterion for bulk metallic glasses. *J Mater Res.* 2006. <https://doi.org/10.1557/jmr.2006.0124>.
- Ashby M, Greer A. Metallic glasses as structural materials. *Scripta Mater.* 2006. <https://doi.org/10.1016/j.scriptamat.2005.09.051>.
- Jiang S-S, Huang Y-J, Wu F-F, Xue P, Sun J-F. A CuZr-based bulk metallic glass composite with excellent mechanical properties by optimizing microstructure. *J Non-Cryst Solids.* 2018. <https://doi.org/10.1016/j.jnoncrystol.2018.01.006>.
- Ning Z, Liang W, Zhang M, Li Z, Sun H, Liu A, Sun J. High tensile plasticity and strength of a cuzr-based bulk metallic glass composite. *Mater Des.* 2016. <https://doi.org/10.1016/j.matdes.2015.10.117>.
- Chen Y, Tang C, Jiang J-Z. Bulk metallic glass composites containing B_2 phase. *Prog Mater Sci.* 2021. <https://doi.org/10.1016/j.pmatsci.2021.100799>.
- Taherzadeh Mousavian R, Zavařnik J, Heidarzadeh A, Bahramyan M, Vijayaraghavan R, Mc-Carthy E, Clarkin O, McNally P, Brabazon D. Development of bmg-b₂ nanocomposite structure in haz during laser surface processing of ZrCuNiAlTi bulk metallic glasses. *Appl Surf Sci.* 2020. <https://doi.org/10.1016/j.apsusc.2019.144535>.
- Xu D, Lohwongwatana B, Duan G, Johnson WL, Garland C. Bulk metallic glass formation in binary Cu-rich alloy series $\text{Cu}_{100-x}\text{Zr}_x$ ($x=34, 36, 38.2, 40$ at) and mechanical properties of bulk cu64zr36 glass. *Acta Mater.* 2004. <https://doi.org/10.1016/j.actamat.2004.02.009>.
- Wang D, Li Y, Sun BB, Sui ML, Lu K, Ma E. Bulk metallic glass formation in the binary Cu–Zr system. *Appl Phys Lett.* 2004. <https://doi.org/10.1063/1.1751219>.
- Wang W, Lewandowski J, Greer A. Understanding the glass-forming ability of $\text{Cu}_{50}\text{Zr}_{50}$ alloys in terms of a metastable eutectic. *J Mater Res.* 2005. <https://doi.org/10.1557/jmr.2005.0302>.
- Li Y, Guo Q, Kalb JA, Thompson CV. Matching glass-forming ability with the density of the amorphous phase. *Science.* 2008;322(5909):1816–9. <https://doi.org/10.1126/science.1163062>.
- Yang L, Guo GQ, Chen LY, Huang CL, Ge T, Chen D, Liaw PK, Saksl K, Ren Y, Zeng QS, La Qua B, Chen FG, Jiang JZ. Atomic scale mechanisms of the glass-forming ability in metallic glasses. *Phys Rev Lett.* 2012. <https://doi.org/10.1103/PhysRevLett.109.105502>.
- Koval Y, Firstov G, Kotko A. Martensitic transformation and shape memory effect in ZrCu intermetallic compound. *Script Metall Mater.* 1992. [https://doi.org/10.1016/0956-716X\(92\)90153-6](https://doi.org/10.1016/0956-716X(92)90153-6).
- Pauly S, Liu G, Wang G, Kuhn U, Mattern N, Eckert J. Microstructural heterogeneities governing the deformation of $\text{Cu}_{47.5}\text{Zr}_{47.5}\text{Al}_5$ bulk metallic glass composites. *Acta Mater.* 2009. <https://doi.org/10.1016/j.actamat.2009.07.042>.
- Hofmann DC. Shape memory bulk metallic glass composites. *Science.* 2010. <https://doi.org/10.1126/science.1193522>.
- Song K, Pauly S, Zhang Y, Gargarella P, Li R, Barekar N, Kuhn U, Stoica M, Eckert J. Strategy for pinpointing the formation of B_2 CuZr in metastable CuZr-based shape memory alloys. *Acta Mater.* 2011. <https://doi.org/10.1016/j.actamat.2011.07.017>.
- Kim BJ, Yun YS, Kim WT, Kim DH. Phase formation and mechanical properties of Cu–Zr–Ti bulk metallic glass composites. *Metals Mater Int.* 2016. <https://doi.org/10.1007/s12540-016-6386-x>.
- Zhang T, Men H, Pang S, Fu J, Ma C, Inoue. Effects of a minor addition of Si and/or Sn on formation and mechanical properties of Cu–Zr–Ti bulk metallic glass. *Mater Sci Eng: A.* 2007. <https://doi.org/10.1016/j.msea.2005.12.102>.
- Friedman HL. Kinetics of thermal degradation of char-forming plastics from thermogravimetry. *J Polym Sci Part C: Polym Symp.* 1964;6(1):183–5.
- Takeo O. A new method of analysis thermogravimetric data. *Bull Chem Soc Jpn.* 1965;38:1881–6. <https://doi.org/10.1246/bcsj.38.1881>.
- T. Velikanova, M. Turchanin. Cu-Ti-Zr (copper- titanium-zirconium): Datasheet from Landolt-Bornstein group IV physical chemistry volume 11c3: “non-ferrous metal systems. part 3” in springer materials, doi:<https://doi.org/10.1007/978-3-540-47004-5>, copyright 2007 Springer Verlag Berlin Heidelberg.
- Kalay I, Kramer MJ, Napolitano RE. High- accuracy x-ray diffraction analysis of phase evolution sequence during devitrification of $\text{Cu}_{50}\text{Zr}_{50}$ metallic glass. *Metall Mater Trans.* 2011. <https://doi.org/10.1007/s11661-010-0531-9>.
- Pauly S, Das J, Mattern N, Kim D, Eckert J. Phase formation and thermal stability in Cu–Zr–Ti(Al) metallic glasses. *Intermetallics.* 2009. <https://doi.org/10.1016/j.intermet.2008.12.003>.
- Pauly S, Das J, Bednarcik J, Mattern N, Kim K, Kim D, Eckert J. Deformation-induced martensitic transformation in Cu–Zr–(Al, Ti) bulk metallic glass composites. *Scripta Mater.* 2009. <https://doi.org/10.1016/j.scriptamat.2008.11.015>.
- Pauly S, Das J, Duhamel C, Eckert J. Effect of titanium on microstructure and mechanical properties of $\text{Cu}_{50}\text{Zr}_{50}\text{Ti}_x$ ($2.5 \leq x \leq 7.5$) glass matrix composites. *Metall Mater Trans.* 2008. <https://doi.org/10.1007/s11661-007-9291-6>.
- Reckendorf RMZ, Schmidt PC, Weiss A. The ternary systems Cu-Ti-Al and Cu-Zr-Al around the Heusler phase composition Cu_2xAl ($x = \text{Ti, Zr}$: phase diagrams and hydrogen solubility. *J Less Common Metals.* 1990. [https://doi.org/10.1016/0022-5088\(90\)90155-D](https://doi.org/10.1016/0022-5088(90)90155-D).
- Hermana GN, Hsiao H-M, Kuo P-C, Liaw PK, Li Y-C, Iikubo S, Yen Y-W. Phase equilibria of the Cu-Zr-Ti ternary system at 703 °C and the thermodynamic assessment and metallic glass region prediction of the Cu-Zr-Ti ternary system. *J Non-Cryst Solids.* 2021. <https://doi.org/10.1016/j.jnoncrystol.2020.120387>.

35. Stein F, Leineweber A. Laves phases: a review of their functional and structural applications and an improved fundamental understanding of stability and properties. *J Mater Sci.* 2021. <https://doi.org/10.1007/s10853-020-05509-2>.

Publisher's Note Springer Nature remains neutral with regard to jurisdictional claims in published maps and institutional affiliations.

Springer Nature or its licensor (e.g. a society or other partner) holds exclusive rights to this article under a publishing agreement with the author(s) or other rightsholder(s); author self-archiving of the accepted manuscript version of this article is solely governed by the terms of such publishing agreement and applicable law.